

Improved Corrosion Resistance of Galvanized Steel with a Zinc Phosphate Coating in Alkaline Solution

De-lin Lai^{1,*}, Yan-bin Jiang¹, Yan-qi Wang², Gang Kong², Chun-shan Che²

¹ School of Chemistry and Chemical Engineering, South China University of Technology, Guangzhou 510640, China;

² School of Materials and Science Engineering, South China University of Technology, Guangzhou 510640, China;)

*E-mail: flyaaa01@163.com

Received: 3 February 2020 / Accepted: 7 April 2020 / Published: 10 May 2020

The corrosion activity of a zinc phosphate coating (ZP layer) on galvanized steel (GS) in alkaline solution in the presence of Ca^{2+} was investigated using open-circuit potential (OCP), potentiodynamic polarization (PDP) and electrochemical impedance spectroscopy (EIS) techniques. The results showed that, compared to that for the bare GS, the phosphate-coated GS presented a robust resistance to corrosion in a saturated $\text{Ca}(\text{OH})_2$ solution with/without 0.5 M chloride. The GS pretreated with the phosphate coating was conducive to suppressing the rapid dissolution of the zinc layer and hydrogen evolution in the alkaline solution. The presence of Ca^{2+} in alkaline solution was beneficial to inhibit the dissolution of the ZP layer by precipitating calcium hydroxyzincate ($\text{Ca}(\text{Zn}(\text{OH})_3)_2 \cdot 2\text{H}_2\text{O}$) and hydroxyapatite ($\text{Ca}_{10}(\text{PO}_4)_6(\text{OH})_2$) at the corroding interface to form an effective barrier film.

Keywords: galvanized coating; phosphate coating; alkaline corrosion

1. INTRODUCTION

Reinforced concrete structures (RCSs) are widely used for construction because of their multifunctionality and relatively low cost [1]. It is believed that the steel can remain passive in concrete thanks to a stable oxide layer formed on its surface in a highly alkaline concrete environment [2]. However, the presence of chloride and concrete carbonation can aggravate the corrosion of steel, which can cause severe damage to RCSs and seriously shorten their service life [3, 4]. Among the recent protection methods for preventing corrosion of the steel in concrete, it has been suggested that the use of hot-dip galvanization is an effective measure to prolong the service life of RCSs [5, 6]. Hot-dip galvanized steel is corroded at an acceptably low rate in alkaline concrete environments due to a compact passivation film formed on the surface of the zinc layer [5-10]. The lowest chloride ion concentrations

cause corrosion of the galvanized steel, which is several times higher than that of the steel in concrete [5, 6, 11].

However, when a hot-dip galvanized coating is embedded in wet concrete, rapid dissolution of the zinc layer and hydrogen evolution occur, which could result in a certain amount of consumption of the zinc layer and loss of adherence between the galvanized steel and concrete [3, 4, 12-16]. To prevent rapid corrosion of the zinc layer and hydrogen evolution, Cr(VI) species have traditionally been employed as conversion coatings and active inhibitors for hot-dip galvanized coatings [4, 17]. However, due to health and environmental considerations, environmentally friendly replacements have been proposed. For instance, galvanized steel pretreated with conversion coatings based on rare earth salts or sol-gel coatings before it has been immersed in a simulated concrete environment have been reported [3, 4, 12-14, 18, 19].

Zinc phosphate coatings are one of the most widely used chromium-free conversion coatings for preventing corrosion of galvanized steel and other metals in neutral chloride environments [20-24]. However, studies on the corrosion activity of zinc phosphate coatings in alkaline solutions are limited [25, 26]. K. Ogle et al. found that in 0.1 M NaOH solution, phosphate and zinc were removed in a 1:1 ratio, and phosphate leaching was reduced in the presence of Mn^{2+} , Fe^{2+} , or Ni^{2+} ions in the phosphate layer [26]. The study by Hassane Idrissi et al. suggested that phosphated mild steel was more resistant than mild steel alone in $Ca(OH)_2$ solution with and without chloride [27, 28]. However, the corrosion activity of zinc phosphate coatings on hot-dip galvanized coatings in alkaline solutions in the presence of Ca^{2+} is not currently available. Consequently, to further improve the corrosion resistance of GS in an alkaline concrete environment, this paper aims to develop a zinc phosphate coating on the galvanized steel to study its inhibition of the rapid corrosion of the zinc layer and hydrogen evolution in a saturated $Ca(OH)_2$ solution that simulates concrete pore solution with and without chloride.

2. EXPERIMENTAL METHODS

2.1. Materials and Exposure Conditions

Table 1. Chemical composition (wt%) of Q235 cold rolled steel sheet.

Element	C	Si	P	Al	Mn	Cr	S	Ni	Fe
wt%	0.038	0.03	0.012	0.01	0.21	0.01	0.01	0.01	Balance

A Q235 cold rolled steel sheet with dimensions of 40 mm × 30 mm × 0.6 mm was chosen as the substrate for the galvanized coating, and the composition of the substrate is listed in Table 1. The steel sheet was pretreated as described previously [29] then hot-dip galvanized at 450°C for 1 min and cooled by water. The zinc phosphate coating was generated in a solution at room temperature for 30 min and then dried at room temperature overnight. The solution was prepared by the addition of zinc oxide ZnO (1.2 g/L), sodium nitrate (15 g/L), 5 ml/L hydrogen peroxide (H_2O_2) and 85% phosphoric acid (H_3PO_4)

(11 ml/L) in distilled water, and the pH was adjusted to 3.0 with NaOH. The specimens (bare GS, phosphated GS) were mounted in epoxy resin, where an exposed area of 2 cm² was left. The bare GS samples were degreased with ethanol by ultrasonication, cleaned carefully with distilled water and dried before testing.

A saturated Ca(OH)₂ solution was used to simulate concrete pore solution [7, 14]. The exposed solution was kept with a constant volume (1000 ml) in a plastic beaker. To simulate marine exposure, Cl⁻ was added as NaCl at concentrations of 0.5 M (seawater) [30]. The experiment was performed at 20 ± 2 °C. The samples (bare GS) immersed in the alkaline solutions without and with chloride were labelled as Z and ZC, respectively, and the samples (phosphated GS) immersed in the alkaline solutions without and with chloride were labelled as ZP and ZPC, respectively.

2.2. Characterization methods

A CHI660E potentiostat with a three-electrode cell was used for the electrochemical tests and consisted of a saturated calomel electrode as the reference electrode, a platinum sheet (8 cm² in size) as the counter electrode and the specimens as the working electrode. The open-circuit potential (OCP) was recorded as a function of exposure time at regular intervals for up to 9 days of immersion. Potentiodynamic polarization curves were measured with a scan rate of 0.1 mV/s. EIS spectra were obtained in a frequency range of 10⁵ Hz to 10⁻² Hz at corrosion potential with amplitude of 10 mV. The impedance data were analysed using ZSimpWin 3.3 software.

Scanning electron microscopy (SEM) with a Quanta 200 microscope equipped with energy dispersive X-ray spectroscopy (EDS) was used to characterize the morphology and elemental composition of the corrosion products. The corrosion products were also characterized by X-ray diffraction (XRD) using Cu K α radiation with a counting time of 0.1 s/step, angular resolution of 0.02°, and angular range of 10-80° (2 θ).

3. RESULTS

3.1. Morphology and composition of the coating

Fig. 1 shows the morphology and XRD patterns of the zinc phosphate coating used in the present work. In Fig. 1a, it can be seen that the zinc phosphate coating is compact and completely covers the steel sheet. The XRD patterns in Fig. 1b indicate the presence of two phases: hopeite (Zn₃(PO₄)₂·4H₂O) and metallic zinc, which implies that the coating is mainly composed of hopeite (Zn₃(PO₄)₂·4H₂O).

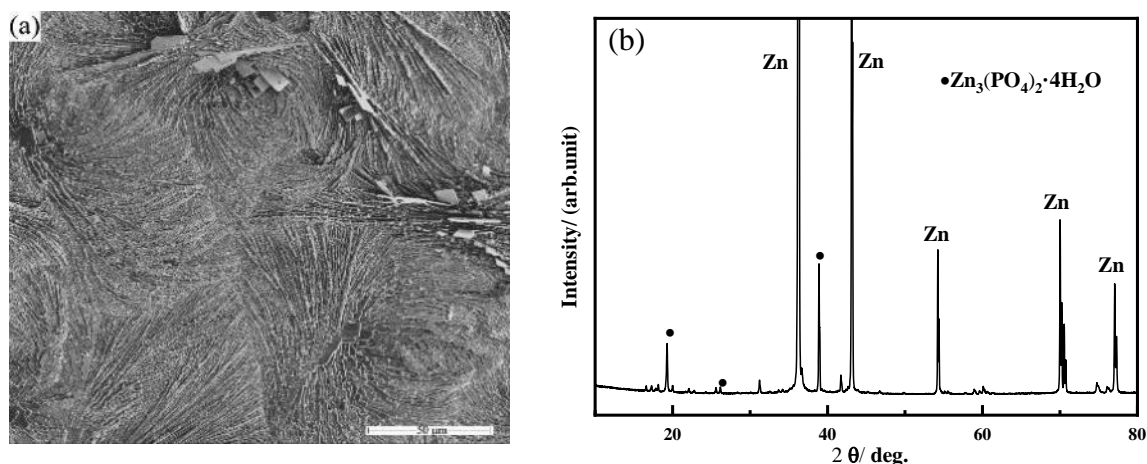


Figure 1. The SEM morphology (a) and XRD patterns (b) of the zinc phosphate coating used in the paper.

3.2. Corrosion behaviour in saturated $\text{Ca}(\text{OH})_2$ solution (S solution)

3.2.1. Electrochemical study

Fig. 2 shows the evolution of the OCP as a function of immersion time. One can observe that the OCP of sample ZP increases gradually with prolonged immersion time and then reaches a relatively constant value after one day of immersion. However, the OCP of sample Z shifts in the negative direction before one day of immersion and then increases gradually to a relatively constant value after 7 days of immersion. Moreover, sample ZP shows a more noble OCP than that of sample Z before 7 days of immersion, and the values of the OCP for samples Z and ZP are almost similar after 7 days of immersion. The registered value of the OCP for sample ZP is larger than -1000 mV vs SCE during the exposure test, which is beneficial to inhibit hydrogen evolution in the alkaline solution with a pH of approximately 12.6 [6, 13]. However, the value of the OCP for sample Z is below -1000 mV vs SCE before 7 days of immersion, which indicates that hydrogen evolution of sample Z likely occurred before 7 days of immersion.

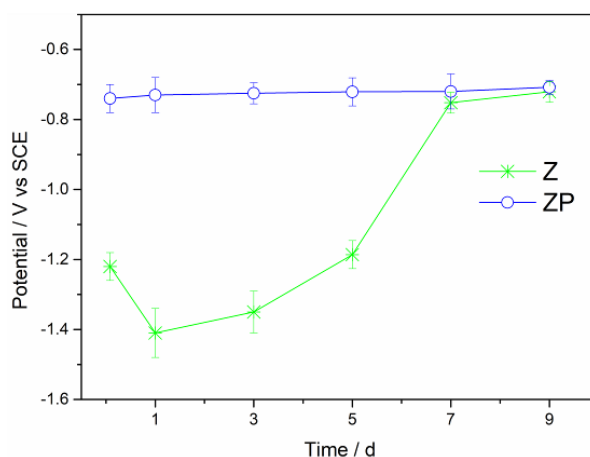


Figure 2. The change in the open-circuit potential for samples Z and ZP as a function of immersion time.

Fig. 3 represents the representative EIS spectra of samples Z and ZP obtained for 2 h and 9 days of immersion. The equivalent circuit models (EC1 and EC2) shown in Fig. 4a and b were used to fit the experimental data, which gave satisfactory results. In the EC1 model, R_s corresponds to the solution resistance, where Q_1 and R_1 represent the capacitance and resistance of the phosphate coating, respectively, and Q_2 and R_2 represent the double-layer capacitance and the charge transfer resistance of the zinc/solution interface, respectively. In the EC2 model, R_s corresponds to the solution resistance, Q is the constant phase element related to the interface phenomenon (electrochemical double layer and/or corrosion product layer) and R is an image of the corrosion resistance of the metallic surface. The equivalent circuit model EC1 was used to fit the EIS spectra for samples Z (after 9 days of immersion) and ZP (after 2 h and 9 days of immersion). The EC2 model was used to fit the EIS spectra for sample Z after 2 h of immersion. Table 2 shows the fitting results of the EIS spectra for samples Z and ZP. The standard deviations of the three specimens are given in Table 2.

In Table 2, R_s has a value range from 38–45 $\Omega \text{ cm}^2$. The impedance at low frequencies is usually interpreted as the polarization resistance R_p , which is inversely proportional to the corrosion rate. A high polarization resistance corresponds to an increased corrosion resistance. The polarization resistance R_p can be obtained by the sum of $R_1 + R_2$. Note that if there is one resistance, which is the charge-transfer resistance R , R_p is equal to the charge-transfer resistance R [31]. In Table 2, in the case of sample Z, the value of R_p remarkably increases from 2 h immersion to 9 days of immersion, which is due to the formation of the passivation film on the sample surface[5-7, 10]. For sample ZP, the value of R_p decreases from 2 h immersion to 9 days of immersion. However, it can be seen that the value of R_p for sample ZP is significantly larger than the value of R_p for sample Z after 2 h of immersion, which indicates that sample ZP obviously has a higher corrosion resistance than that of sample Z during the initial corrosion process. Again, for 9 days of immersion, sample ZP also has a higher R_p than that of sample Z, which also implies that sample ZP has a higher corrosion resistance than sample Z after a long immersion time. It can be concluded that the corrosion resistance of the galvanized steel in the alkaline solution is remarkably improved by pretreatment with the zinc phosphate coating. In addition, one can observe that the corrosion resistance of the zinc phosphate coating is higher than that of the passivation film formed on the surface of sample Z.

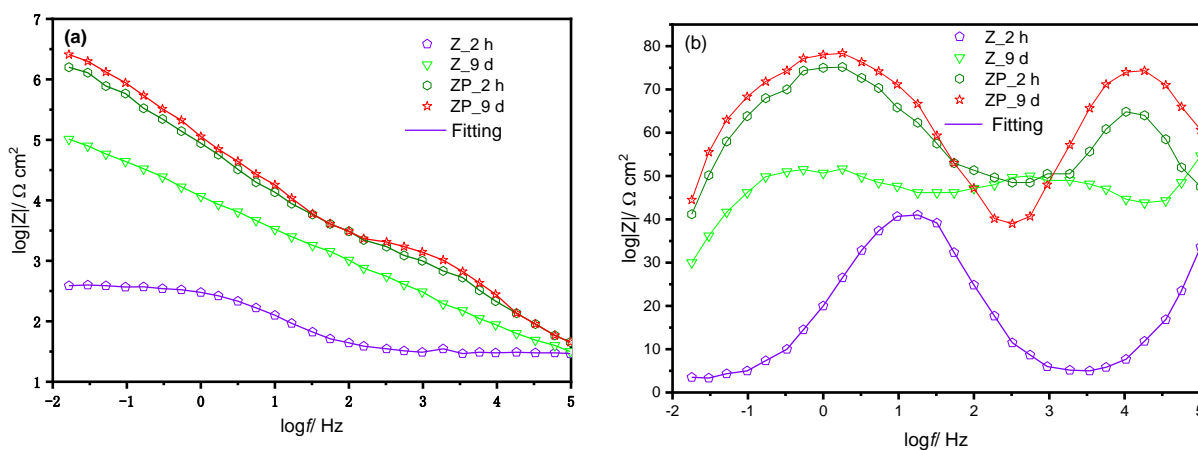


Figure 3. Representative EIS spectra for samples Z and ZP obtained after 2 h and 9 days of immersion.

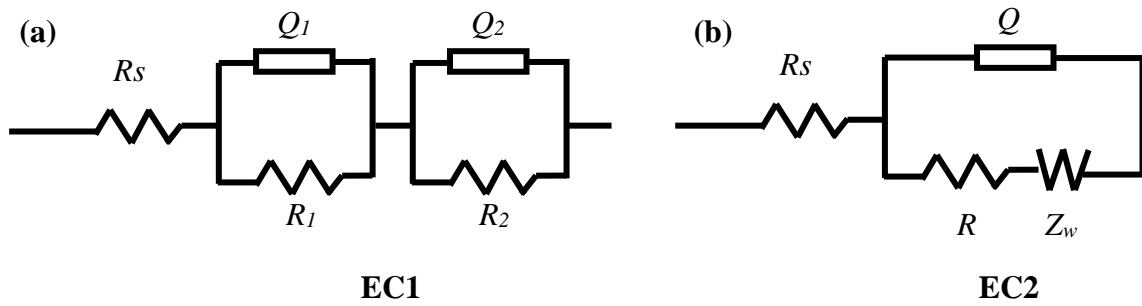


Figure 4. Equivalent circuit used for modelling the EIS data.

Table 2. Electrical parameters for samples Z and ZP immersed in S solution obtained through fitting EIS data; the standard deviations from 3 specimens are given.

Sample	R/R_1 ($\Omega \text{ cm}^2$)	Q/Q_1 10^{-6} (S sn cm^{-2})	n_1	Z_w ($\Omega \text{ cm}^2$)	R_2 ($\text{k}\Omega \text{ cm}^2$)	Q_2 10^{-6} (S sn cm^2)	n_2	R_p ($\text{k}\Omega \text{ cm}^2$)
Z_2h	324 ± 45	141 ± 11	0.62 ± 0.11	0.17 ± 0.06	-	-	-	0.32
Z_9d	708 ± 64	31 ± 9	0.75 ± 0.12	-	155 ± 14	3.1 ± 0.6	0.69 ± 0.12	155
ZP_2h	1592 ± 265	2.1 ± 0.7	0.85 ± 0.14	-	3903 ± 326	0.3 ± 0.08	0.91 ± 0.07	3904
ZP_9d	1439 ± 248	2.5 ± 0.6	0.75 ± 0.08	-	2478 ± 256	2.9 ± 0.5	0.81 ± 0.08	2479

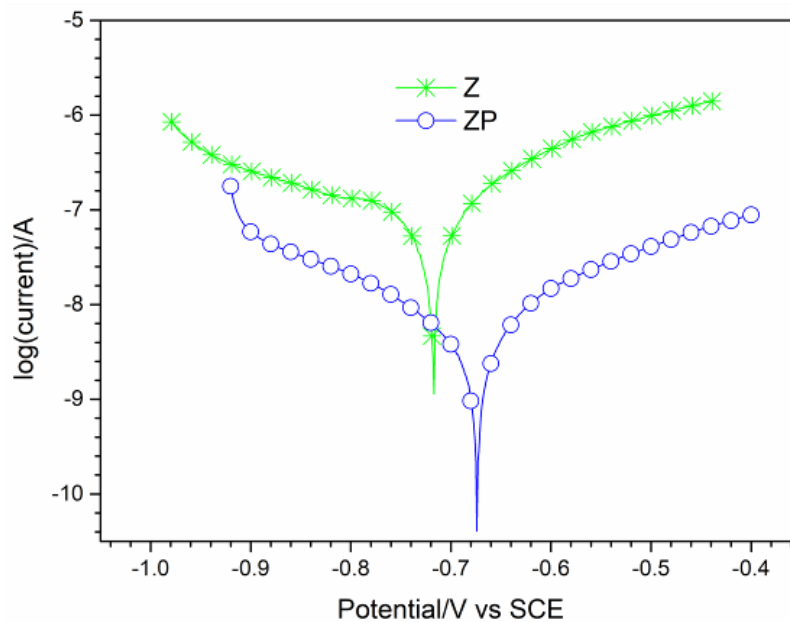


Figure 5. Representative polarization curves for sample Z and ZP after 9 days of immersion in saturated $\text{Ca}(\text{OH})_2$ solution.

Fig. 5 shows the representative polarization curves of samples Z and ZP obtained after 9 days of immersion. The corrosion current I_{corr} for samples Z and ZP can be obtained by the Tafel extrapolation method [7, 32]. The corrosion current I_{corr} , corrosion potential E_{corr} , and Tafel slopes b_a and b_c are listed

in Table 3. In Table 3, it can be observed that sample ZP also shows a lower corrosion rate than sample Z after 9 days of immersion, which agrees with the results obtained from the EIS study.

Table 3. I_{corr} , E_{corr} , and Tafel slopes b_a and b_c obtained for samples Z and ZP after 9 days of immersion in the S solution; the standard deviations from 3 specimens are given.

Sample	E_{corr}/V (vs SCE)	I_{corr} ($\mu\text{A}/\text{cm}^2$)	b_a (mV/decade)	$-b_c$ (mV/decade)
Z	-0.717 ± 0.023	0.16 ± 0.04	177 ± 24	299 ± 24
ZP	-0.701 ± 0.016	0.08 ± 0.01	189 ± 31	233 ± 31

3.2.2. SEM analysis

Fig. 6 shows the SEM images and XRD patterns of the corrosion products for samples Z and ZP after 9 days of immersion. In Fig. 6a, a compact plate-like corrosion product completely covers sample Z. The XRD analysis in Fig. 6c shows that the plate-like corrosion products are mainly composed of calcium hydroxyzincate ($\text{Ca}(\text{Zn}(\text{OH})_3)_2 \cdot 2\text{H}_2\text{O}$), which is in agreement with the results in Ref. [6, 7, 33-36]. In Fig. 6b, it can be seen that the surface of sample ZP is also completely covered by a compact layer. The XRD analysis in Fig. 6c shows that the dense layer mainly consists of hopeite ($\text{Zn}_3(\text{PO}_4)_2 \cdot 4\text{H}_2\text{O}$), calcium hydroxyzincate ($\text{Ca}(\text{Zn}(\text{OH})_3)_2 \cdot 2\text{H}_2\text{O}$) and hydroxyapatite ($\text{Ca}_{10}(\text{PO}_4)_6(\text{OH})_2$). In addition, compared to the SEM morphology of the zinc phosphate coating in Fig. 1a, one can observe that a change in the morphology in Fig. 6b takes place after 9 days of immersion in saturated $\text{Ca}(\text{OH})_2$ solution.

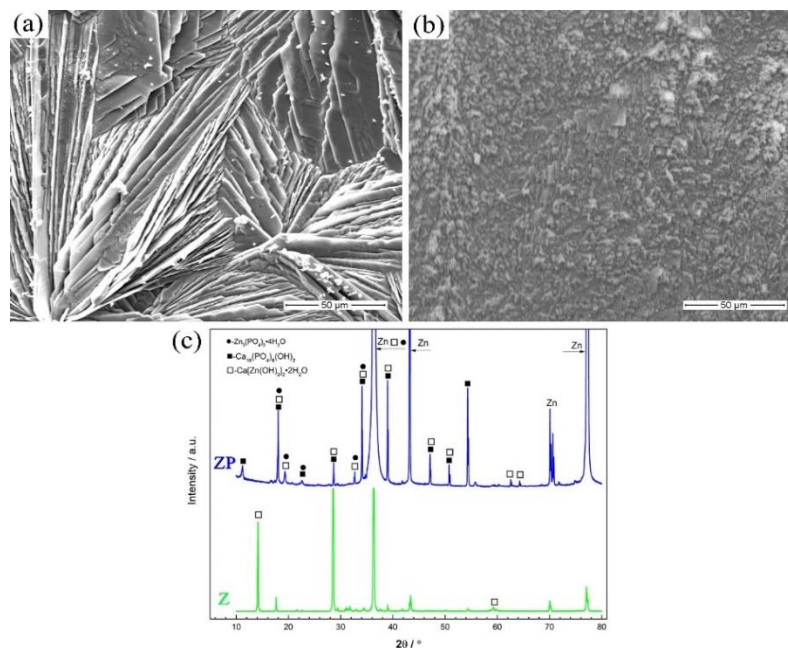


Figure 6. SEM image and XRD patterns (c) obtained after 9 days of immersion for samples: a) Z and b) ZP.

Fig. 7a presents an SEM image and its corresponding elemental maps (shown in Figs. 7b-e) for sample ZP obtained after 9 days of immersion. Figs. 7b-e show the distribution of the elements O, Ca, P and Zn, respectively. As seen in Figs. 7b-c, the elements O, Ca, P and Zn are distributed evenly on the surface of sample ZP. Notably, the existence of Ca implies the formation of Ca-containing corrosion products after sample ZP is immersed in the alkaline solution in the presence of Ca^{2+} . It can be concluded that a composite barrier film containing Ca, O, P and Zn forms on the surface of sample ZP when immersed in the alkaline solution. The result is consistent with that obtained from XRD analysis in Fig. 6c.

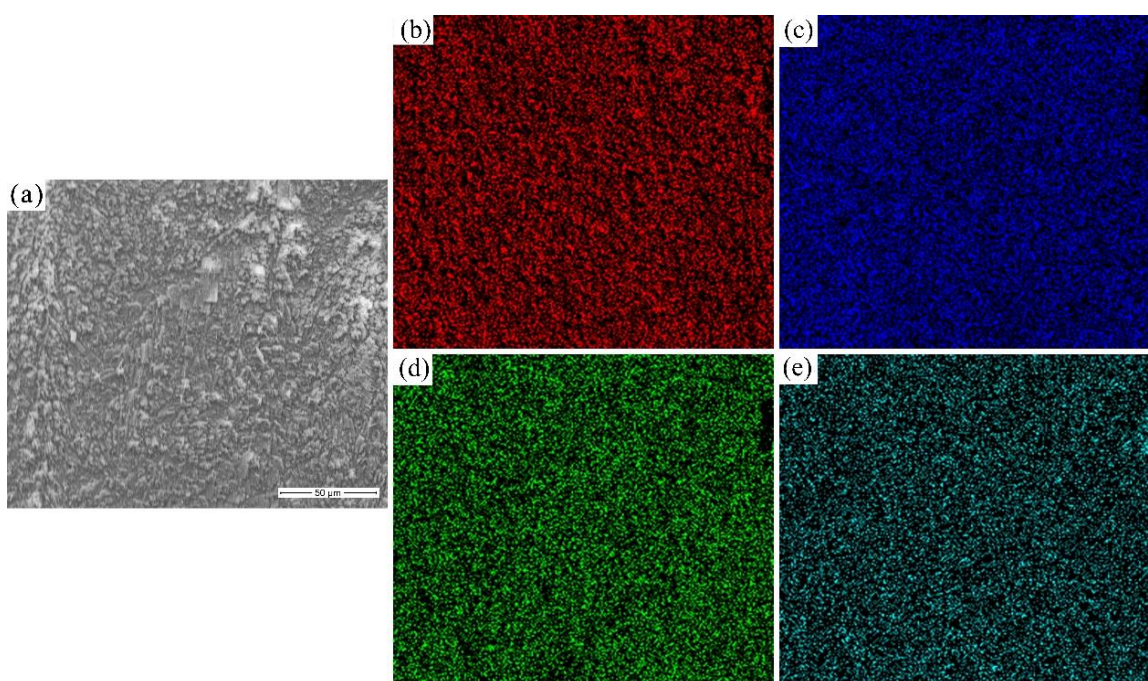


Figure 7. SEM morphology (a) and its corresponding elemental maps: b) O, c) Ca, d) P and e) Zn for sample ZP obtained after 9 days of immersion in saturated $\text{Ca}(\text{OH})_2$ solution.

3.3. Corrosion behaviour in the saturated $\text{Ca}(\text{OH})_2$ solution contaminated by chloride (SC)

3.3.1. Electrochemical study

Fig. 8 shows the evolution of the collected OCP as a function of immersion time. The OCP of sample ZPC increases gradually with prolonged immersion time and then reaches a relatively constant value after 7 days of immersion. The OCP of sample ZC shifts in the negative direction before one day of immersion and then increases gradually to a relatively constant value after 7 days of immersion. Moreover, sample ZPC shows a more noble OCP than that of sample ZC during the whole immersion test. The collected OCP for sample ZPC is above -1000 mV vs SCE during the whole test, which is also conducive to suppressing hydrogen evolution in the alkaline solution with a pH of approximately 12.6 [6, 13]. However, the value of the OCP for sample ZC is below -1000 mV vs SCE during the whole

exposure test, which indicates that hydrogen evolution of sample ZC likely occurs in the saturated $\text{Ca}(\text{OH})_2$ solution contaminated by chloride.

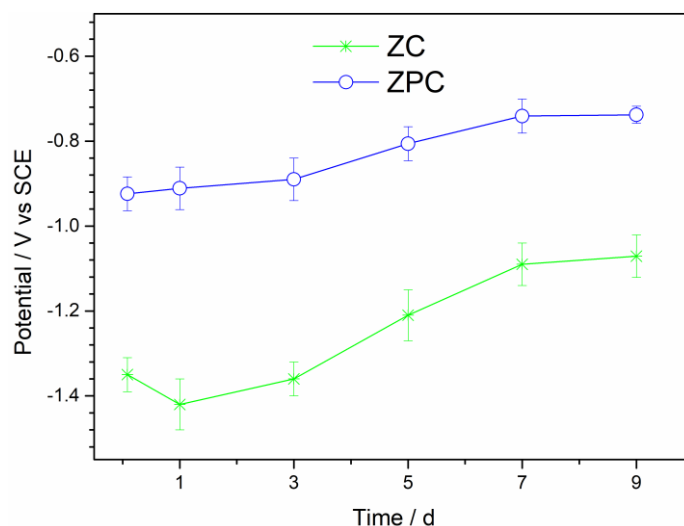


Figure 8. The evolution of the open circuit potential for samples ZC and ZPC as a function of immersion time.

Fig. 9 represents the representative EIS spectra of samples Z and ZP obtained for 2 h and 9 days of immersion. The equivalent circuit models (EC1 and EC2) shown in Figs. 4a and b were used to fit the experimental data, which gave satisfactory results. The equivalent circuit model EC1 was used to fit the EIS spectra of sample ZPC after 2 h and 9 days of immersion. The EC2 model was used to fit the EIS spectra of sample Z after 2 h and 9 days of immersion. Table 4 shows the fitting results of the EIS spectra for samples Z and ZP. The standard deviations of the three specimens are given in Table 4.

As shown in Table 4, R_s ranges from 11-14 $\Omega \text{ cm}^2$. For sample ZC, the value of R_p increases with prolonged immersion time, which is mainly due to the formation of the passivation film on the sample surface [5-7, 10]. In the case of sample ZPC, the value of R_p decreases slightly from 2 h immersion to 9 days of immersion. However, it can be seen that the value of R_p for sample ZPC is significantly larger than that for sample ZC after 2 h of immersion, which indicates that sample ZPC obviously has a higher corrosion resistance than sample ZC during the initial corrosion process. Again, for 9 days of immersion, sample ZPC also presents higher R_p than sample ZC, which also implies that sample ZPC has a higher corrosion resistance than sample ZC after a long immersion time. It can be concluded that the corrosion resistance of the galvanized steel in the alkaline solution contaminated by chloride was remarkably improved by pretreatment with the zinc phosphate coating.

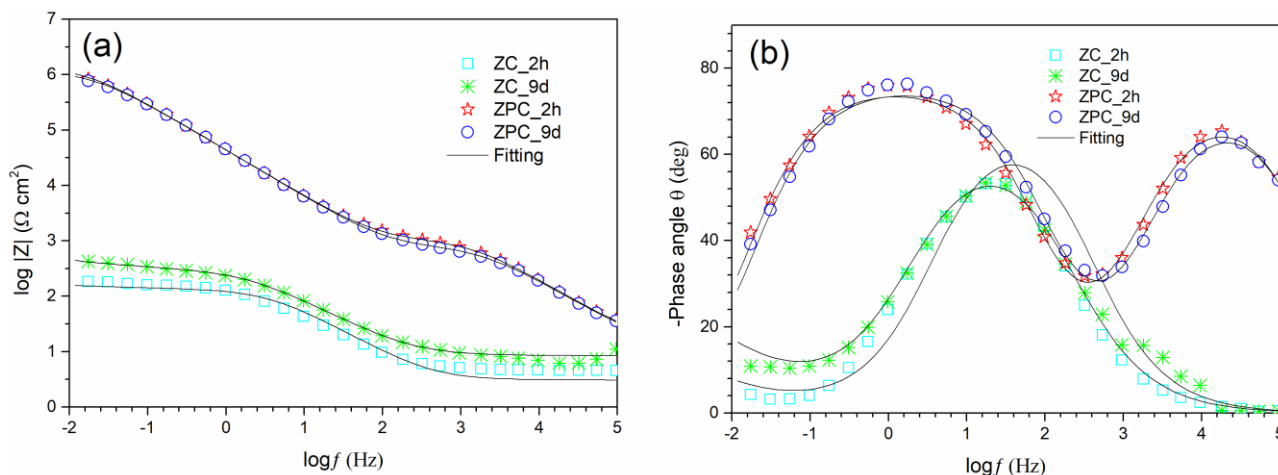


Figure 9. Representative EIS spectra for samples ZC and ZPC obtained after 2 h and 9 days of immersion.

Table 4. Electrical parameters for samples ZC and ZPC immersed in the SC solution obtained by fitting EIS data; the standard deviations for 3 specimens are given.

Samples	R_1 ($\Omega \text{ cm}^2$)	Q_1 10^{-6} (S sn cm^{-2})	n_1	Z_w ($\Omega \text{ cm}^2$)	R_2 ($\text{k}\Omega \text{ cm}^2$)	Q_2 10^{-6} (S sn cm^{-2})	n_2	R_p ($\text{k}\Omega \text{ cm}^2$)
ZC_2h	135 ± 35	574 ± 91	0.64 ± 0.10	0.13 ± 0.04	-	-	-	0.14
ZC_9d	311 ± 49	489 ± 89	0.76 ± 0.15	0.022 ± 0.01	-	-	-	0.31
ZPC_2h	980 ± 104	4.7 ± 0.6	0.84 ± 0.09	-	1435 ± 136	0.5 ± 0.1	0.83 ± 0.07	1436
ZPC_9d	802 ± 93	4.1 ± 0.5	0.84 ± 0.13	-	1212 ± 127	2.3 ± 0.3	0.94 ± 0.05	1213

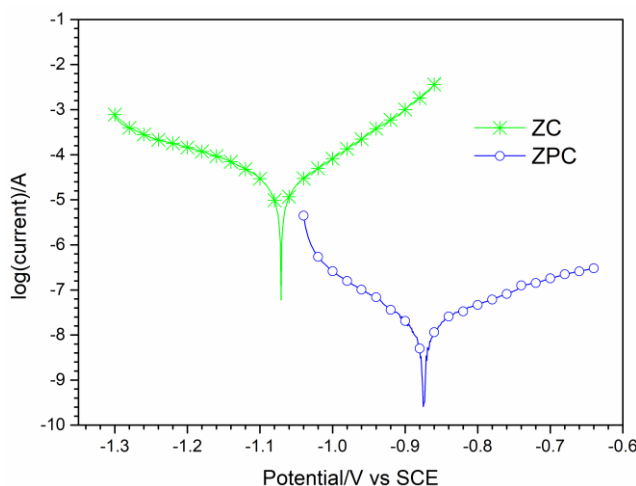


Figure 10. Representative polarization curves for samples ZC and ZPC immersed after 9 days of immersion in saturated $\text{Ca}(\text{OH})_2$ solution contaminated by chloride.

Fig. 9 shows the representative polarization curves of samples ZC and ZPC obtained after 9 days of immersion. The corrosion currents I_{corr} of samples ZC and ZPC were obtained by the Tafel

extrapolation method [7, 32]. The corrosion currents I_{corr} , corrosion potential E_{corr} , and Tafel slopes b_a and b_c are listed in Table 5. In Table 5, it can be observed that sample ZPC also shows a lower corrosion rate than sample ZC after 9 days of immersion, which agrees with the results obtained from the EIS study in Table 4.

Table 5. I_{corr} , E_{corr} , and Tafel slopes b_a and b_c obtained for samples ZC and ZPC after 9 days of immersion in the SC solution; the standard deviations for 3 specimens are given

Sample	E_{corr}/V (vs SCE)	I_{corr} ($\mu\text{A}/\text{cm}^2$)	b_a (mV/decade)	$-b_c$ (mV/decade)
ZC	-1.071 ± 0.025	21.9 ± 3	92 ± 20	97 ± 16
ZPC	-0.738 ± 0.014	0.11 ± 0.01	160 ± 38	250 ± 27

3.3.2. SEM analysis

Fig. 11 depicts the SEM images and XRD patterns of the corrosion products for samples ZC and ZPC after 9 days of immersion. In Fig. 11a, it can be seen that compared to the compact corrosion product layer on sample Z, the corrosion product layer on the surface of sample ZC is porous, and the size of the plate-like corrosion products is larger; thus, sample ZC has a lower corrosion resistance than that of sample Z. The result is in agreement with the result obtained from the electrochemical study in Tables 2-5. In addition, the XRD analysis in Fig. 11c shows that the corrosion products for sample ZC also mainly consist of calcium hydroxyzincate ($\text{Ca}(\text{Zn}(\text{OH})_3)_2 \cdot 2\text{H}_2\text{O}$). In Fig. 11b, one can observe that a compact layer also completely covers sample ZPC. The XRD analysis in Fig. 11c indicates that the dense layer is mainly composed of hopeite ($\text{Zn}_3(\text{PO}_4)_2 \cdot 4\text{H}_2\text{O}$), calcium hydroxyzincate ($\text{Ca}(\text{Zn}(\text{OH})_3)_2 \cdot 2\text{H}_2\text{O}$) and hydroxyapatite ($\text{Ca}_{10}(\text{PO}_4)_6(\text{OH})_2$). Again, compared to the SEM image of the zinc phosphate coating in Fig. 1a, it can be seen that some change of the morphology in Fig. 11b also took place after 9 days of immersion in the saturated $\text{Ca}(\text{OH})_2$ solution contaminated by chloride.

Fig. 12a displays an SEM image and its corresponding elemental maps (shown in Figs. 12b-e) for sample ZPC obtained after 9 days of immersion. Figs. 12b-e present the distribution of the elements O, Ca, P and Zn, respectively. As shown in Figs. 12b-e, the elements O, Ca, P and Zn are also distributed evenly on the surface of sample ZPC. The existence of Ca also indicates that Ca-containing corrosion products formed on the surface of sample ZPC when immersed in the alkaline solution in the presence of Ca^{2+} . The result is consistent with that obtained from the XRD analysis in Fig. 11c.

Fig. 13 shows an SEM image of the cross-sections of the compact composite film for sample ZPC and the corresponding elemental contents obtained after 9 days of immersion. In Fig. 13a, it can be seen that a dense composite film (labelled as the CZP layer in Fig. 13a) has a thickness range from 2-4 μm , which indicates that the zinc phosphate coating was partially dissolved when immersed in the alkaline solution when compared with the results shown in Fig. 1b.

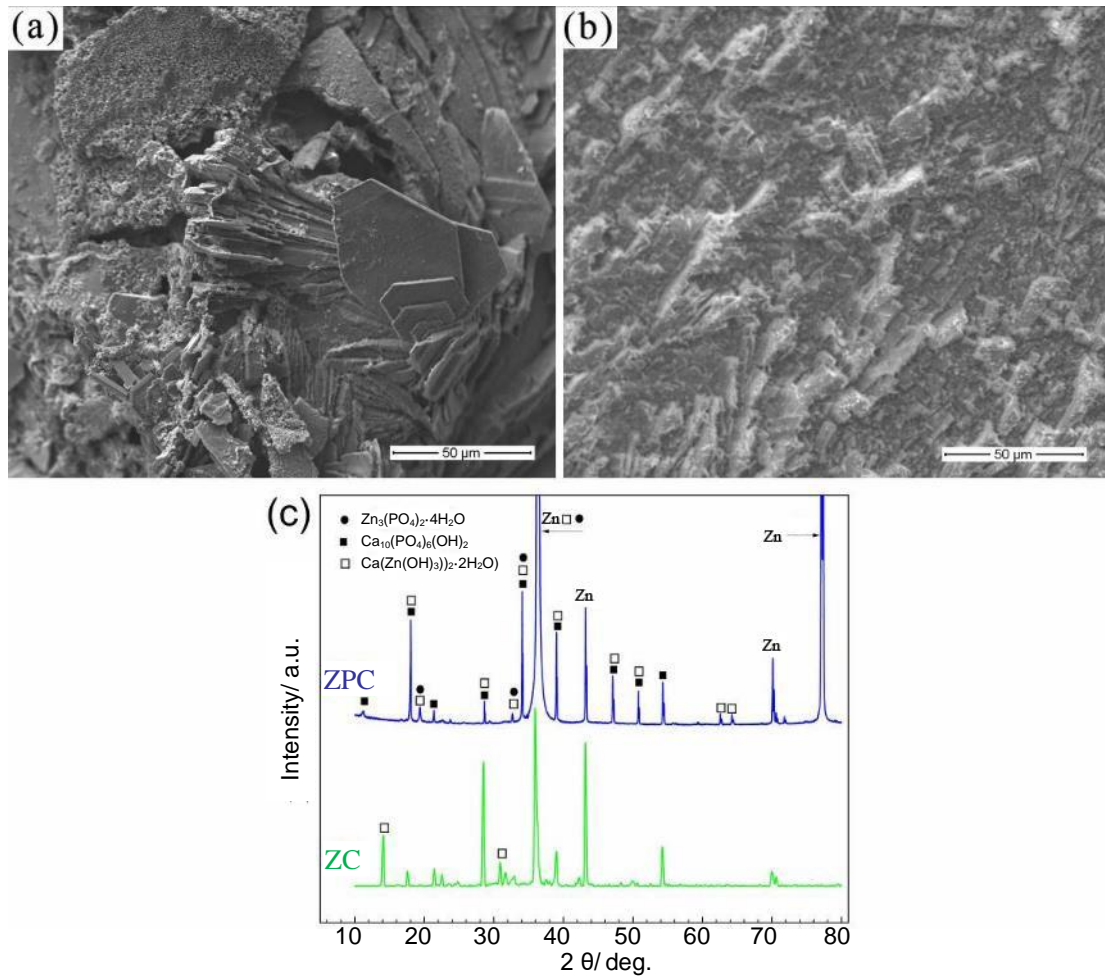


Figure 11. SEM image and XRD patterns (c) obtained after 9 days of immersion for samples: a) ZC and b) ZPC.

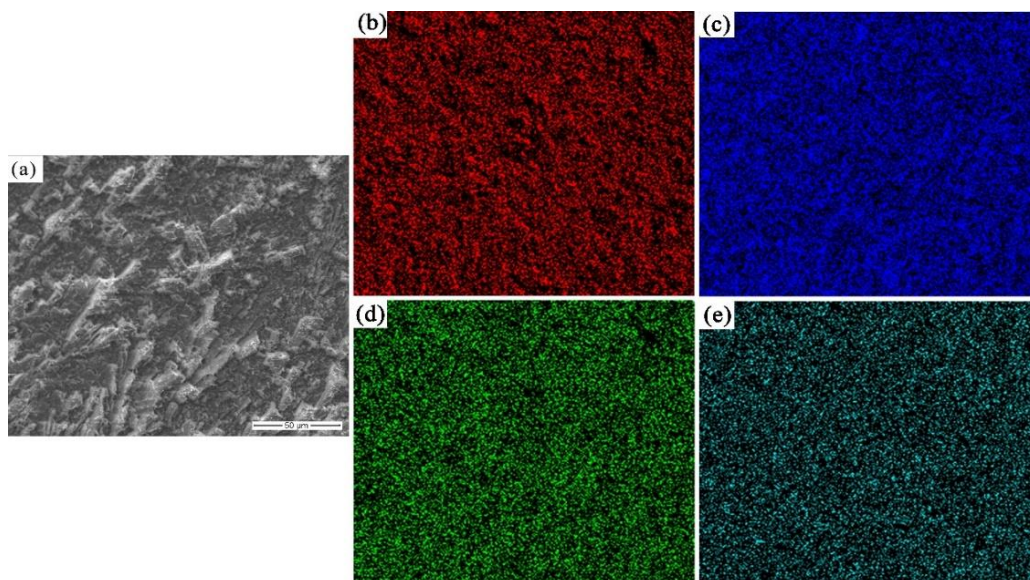


Figure 12. SEM morphology (a) and its corresponding elemental maps: b) O, c) Ca, d) P and e) Zn for sample ZPC obtained after 9 days of immersion in saturated $Ca(OH)_2$ solution contaminated by chloride.

The elemental contents in Fig. 13b show that the dense layer consists of Ca, O, P and Zn, which is consistent with the results obtained from the elemental maps in Figs. 12b-e. In addition, in Fig. 13b, one can see that Ca is mainly distributed on the outer layer of the dense composite film, Zn is mainly distributed on the inner layer of the dense film, and the distribution of P and O is similar.

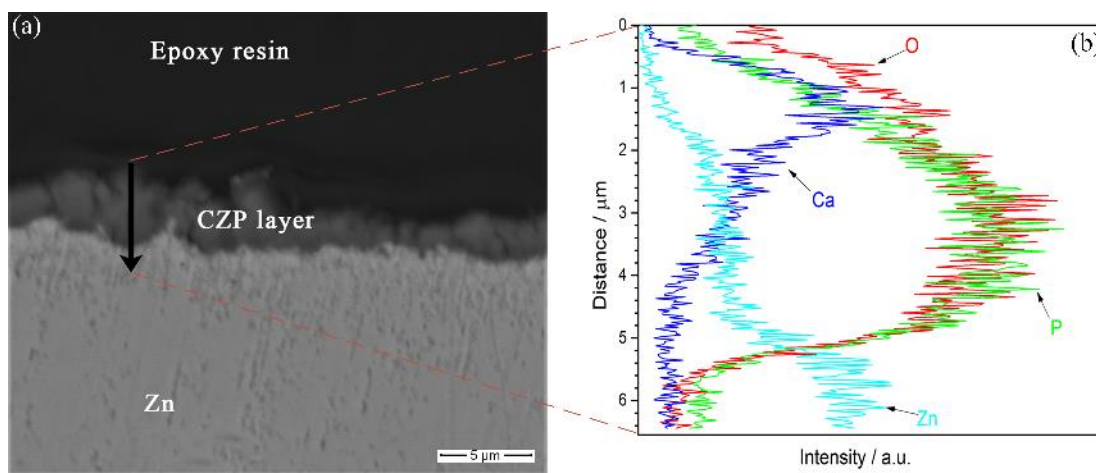


Figure 13. SEM image of the cross-sections of the compact composite film for sample ZPC (a) and corresponding elemental contents (b) obtained after 9 days of immersion.

4. DISCUSSION

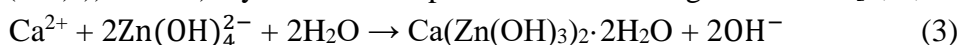
The corrosion behaviour of galvanized steel (GS) in alkaline solutions in the presence of $\text{Ca}(\text{OH})_2$ has been widely studied in recent decades [6, 7, 10, 33, 34, 36-41]. The initial corrosion process of GS mainly involves the active dissolution of the zinc layer and hydrogen evolution according to reactions [6, 15, 16, 42]:



and



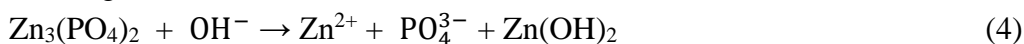
For samples Z and ZC, the evolution of the OCP in Figs. 2 and 8 shows that the active dissolution of the zinc layer and possible hydrogen evolution occurred for several days of immersion in the alkaline solution with a pH of approximately 12.6. However, possible hydrogen evolution of sample ZC may have occurred during the whole test in alkaline solution contaminated by chloride due to a collected OCP lower than -1000 mV vs SCE. The active dissolution of zinc continued with prolonged immersion time until the zincate concentration reached a critical value to precipitate a calcium hydroxyzincate ($\text{Ca}(\text{Zn}(\text{OH})_3)_2 \cdot 2\text{H}_2\text{O}$) layer on the sample surface according to reaction [6, 7, 33]:



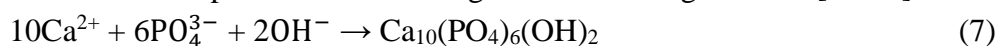
In the case of samples ZP and ZPC, during the initial corrosion process, the zinc phosphate coating on galvanized steel shown in Figs. 1a-b acted as an effective barrier to inhibit the aggressive ion penetration to the metal surface; therefore, samples ZP and ZPC had a remarkably higher corrosion

resistance than samples Z and ZC after 2 h of immersion. On the other hand, in Fig. 2 and Fig. 8, it can be seen that the registered OCP of samples ZP and ZPC was above -1000 mv vs SEC during the test, which implies that the zinc phosphate coating on galvanized steel increased the corrosion potential of the galvanized steel in the alkaline solution. The high corrosion resistance, i.e. the low zinc dissolution rate and noble corrosion potential, suppressed the hydrogen evolution of samples ZP and ZPC during the immersion test [6, 13].

The zinc phosphate coating was unstable and dissolved in the highly alkaline solution according to the following reactions [25, 26]:



Therefore, compared to the original SEM morphology of the phosphate layer in Fig. 1a, the observed change in the SEM morphology of the phosphate layer for samples ZP and ZPC after 9 days of immersion in Fig. 6b and 11b may be partially due to the dissolution of the phosphate layer. The XRD analysis in Figs. 6c and 11c indicates the existence of calcium hydroxyzincate ($\text{Ca}(\text{Zn}(\text{OH})_3)_2 \cdot 2\text{H}_2\text{O}$) and hydroxyapatite ($\text{Ca}_{10}(\text{PO}_4)_6(\text{OH})_2$) in the compact layer on samples ZP and ZPC. In addition, the EDS analysis in Figs. 7, 12-13 implies that calcium hydroxyzincate ($\text{Ca}(\text{Zn}(\text{OH})_3)_2 \cdot 2\text{H}_2\text{O}$) and hydroxyapatite ($\text{Ca}_{10}(\text{PO}_4)_6(\text{OH})_2$) were evenly distributed on the sample surface. In the alkaline solution in the presence of Ca^{2+} , after a certain dissolution of the phosphate layer, as the concentration of zincate and phosphate ions reached a critical value, calcium hydroxyzincate ($\text{Ca}(\text{Zn}(\text{OH})_3)_2 \cdot 2\text{H}_2\text{O}$) was precipitated on the sample surface through reaction (3), and hydroxyapatite ($\text{Ca}_{10}(\text{PO}_4)_6(\text{OH})_2$) was precipitated on the sample surface according to the following reaction [43-45]:



After long immersion times, the precipitation of calcium hydroxyzincate ($\text{Ca}(\text{Zn}(\text{OH})_3)_2 \cdot 2\text{H}_2\text{O}$) and hydroxyapatite ($\text{Ca}_{10}(\text{PO}_4)_6(\text{OH})_2$) at the corroding interface suppressed the further dissolution of the phosphate layer. The resulting composite layer also was an effective barrier and protected the zinc layer from corrosion. Therefore, the electrochemical study in Tables 2-5 shows that samples ZP and ZPC also had a higher corrosion resistance than samples Z and ZC after 9 days of immersion.

4. CONCLUSIONS

The corrosion activity of a zinc phosphate coating on galvanized steel (GS) in a saturated $\text{Ca}(\text{OH})_2$ solution that simulates concrete pore solution was studied using open-circuit potential (OCP), potentiodynamic polarization (PDP) and electrochemical impedance spectroscopy (EIS) techniques. In the early corrosion process, when bare GS was actively corroded with a negative corrosion potential (< -1000 mV vs SEC), phosphated GS had a robust resistance to corrosion in the alkaline solution with/without 0.5 M chloride. GS pre-treated with the phosphate coating was suppressed the rapid dissolution of the zinc layer and hydrogen evolution in the alkaline solution with/without 0.5 M chloride. After long immersion times, when a passivation film formed on the surface of bare GS, the phosphated GS also had a robust resistance to corrosion. The presence of Ca^{2+} in the alkaline solution inhibited the

dissolution of the phosphate coating by precipitating calcium hydroxyzincate ($\text{Ca}(\text{Zn}(\text{OH})_3)_2 \cdot 2\text{H}_2\text{O}$) and hydroxyapatite ($\text{Ca}_{10}(\text{PO}_4)_6(\text{OH})_2$) at the corroding interface to form an effective barrier film after a long immersion time.

ACKNOWLEDGEMENTS

The investigation is supported by the project of the International Lead and Zinc Research Organization.

References

1. Y. Cao, S. Dong, D. Zheng, J. Wang, X. Zhang, R. Du, G. Song, C. Lin, *Corros. Sci.*, 126 (2017) 166-179.
2. H. Luo, H. Su, C. Dong, K. Xiao, X. Li, *Data in brief*, 5 (2015) 171-178.
3. R. B. Figueira, C. J. R. Silva, E. V. Pereira, *J. Electrochem. Soc.*, 162 (2015) 666-676.
4. M. A. Arenas, C. Casado, V. N. Pujol, J. D. Damborenea, *Cem. Concr. Compos.*, 28 (2006) 267-275.
5. S. R. Yeomans, Galvanized steel in concrete: an overview, *Galvanized Steel Reinforcement in Concrete*, (2004), Australia, Elsevier Science.
6. C. Andrade, C. Alonso, Electrochemical aspects of galvanized reinforcement corrosion, *Galvanized Steel Reinforcement in Concrete*, (2004), Spain, Elsevier Science.
7. Y. Q. Wang, G. Kong, C. S. Che, *Corros. Sci.*, 112 (2016) 679-686.
8. A. Macias, C. Andrade, *Brit. Corros. J.*, 22 (1987) 119-129.
9. M. Blanco, C. Andrade, A. Macias, *Brit. Corros. J.*, 19 (1984) 41-48.
10. A. Macias, C. Andrade, *Brit. Corros. J.*, 18 (1983) 82-87.
11. A. Bautista, J. Gonzalez, *Cement Concrete Res.*, 26 (1996) 215-224.
12. R. B. Figueira, C. J. R. Silva, E. V. Pereira, *J. Coat. Technol. Res.*, 13 (2016) 355-373.
13. D. D.N. Singh, R. Ghosh, *Surf. Coat. Tech.*, 202 (2008) 4687-4701.
14. M. Sánchez, M. C. Alonso, P. Cecilio, M. F. Montemor, C. Andrade, *Cem. Concr. Compos.*, 28 (2006) 256-266.
15. P. Pokorný, P. Tej, M. Kouřil, *Constr. Build. Mater.*, 132 (2017) 271-289.
16. R. Pernicova, D. Dobias, P. Pokorny, *Procedia Engineering*, 172 (2017) 859-866.
17. V. Shkirskiy, P. Keil, H. H. Bruening, F. Leroux, T. Stimpfling, D. Dragoie, K. Ogle, P. Volovitch, *Corros. Sci.*, 99 (2015) 31-41.
18. R. B. Figueira, C. J. R. Silva, E. V. Pereira, *Surf. Coat. Tech.*, 265 (2015) 191-204.
19. R. B. Figueira, C. J. R. Silva, E. V. Pereira, *Prog. Org. Coat.*, 88 (2015) 245-255.
20. C. Y. Tsai, J. S. Liu, P. L. Chen, C. S. Lin, *Corros. Sci.*, 52 (2010) 3907-3916.
21. B. L. Lin, J. T. Lu, G. Kong, *Corros. Sci.*, 50 (2008) 962-967.
22. Z. Y. Yong, J. Zhu, C. Qiu, Y. L. Liu, *Appl. Surf. Sci.*, 255 (2008) 1672-1680.
23. A. S. Akhtar, P. C. Wong, K. C. Wong, K. A. R. Mitchell, *Appl. Surf. Sci.*, 254 (2008) 4813-4819.
24. D. Susac, X. Sun, R. Y. Li, K. C. Wong, P. C. Wong, K. A. R. Mitchell. *Appl. Surf. Sci.*, 239 (2004) 45-59.
25. A. Tomandl, M. Wolpers, K. Ogle, *Corros. Sci.*, 46 (2004) 997-1011.
26. K. Ogle, A. Tomandl, N. Meddahi, M. Wolpers, *Corros. Sci.*, 46 (2004) 979-995.
27. F. Simescu, H. Idrissi, *Corros. Sci.*, 51 (2009) 833-840.
28. F. Simescu, H. Idrissi, *Sci. Technol. Adv. Mat.*, 9 (2008) 1-10.
29. S. H. Zhang, G. Kong, J. T. Lu, C. S. Che, L. Y. L., *Surf. Coat. Tech.*, 259 (2014) 654-659.
30. R. D. Moser, P. M. Singh, L. F. Kahn, K. E. Kurtis, *Corros. Sci.*, 57 (2012) 241-253.
31. M. Mouanga, P. Bercot, *Corros. Sci.*, 52 (2010) 3993-4000.

32. L. J. Yang, Y. M. Zhang, X. D. Zeng, Z. L. Song, *Corros. Sci.*, 59 (2012) 229-237.
33. Y. Q. Wang, G. Kong, C. S. Che, T. Y. Weng, Z. W. Sun, *Corros. Sci.*, 136 (2018) 374-385.
34. F. Tittarelli, T. Bellezze, *Corros. Sci.*, 52 (2010) 978-983.
35. Z. Q. Tan, C. M. Hansson, *Corros. Sci.*, 50 (2008) 2512-2522.
36. R. Ghosh, D. D.N. Singh, *Surf. Coat. Tech.*, 201 (2007) 7346-7359.
37. Y. Q. Wang, G. Kong, C. S. Che, B. Zhang, *Constr. Build. Mater.*, 162 (2018) 383-392.
38. G. Roventi, T. Bellezze, E. Barbaresi, R. Fratesi, *Mater. Corros.*, 64 (2013) 1007-1014.
39. T. Bellezze, G. Roventi, E. Barbaresi, N. Ruffini, R. Fratesi, *Mater. Corros.*, 62 (2011) 155-160.
40. A. Macías, C. Andrade, *Cem. Concr. Res.*, 17 (1987) 307-316.
41. A. Macias, C. Andrade, *Brit. Corros. J.*, 22 (1987) 162-171.
42. R. Figueira, C. Silva, E. Pereira, M. Salta, *E. Prot. Mater.*, 33 (2014) 51-61.
43. Y. C. Su, L. Y. Niu, Y. B. Lu, J. S. Lian, G. Y. Li, *J. Electrochem. Soc.*, 160 (2013) C536-C541.
44. X. B. Chen, N. Birbilis, T.B. Abbott, *Corros. Sci.*, 55 (2012) 226-232.
45. R. C. Zeng, Z. D. Lan, L. H. Kong, Y. D. Huang, H. Z. Cui, *Surf. Coat. Tech.*, 205 (2011) 3347-3355

© 2020 The Authors. Published by ESG (www.electrochemsci.org). This article is an open access article distributed under the terms and conditions of the Creative Commons Attribution license (<http://creativecommons.org/licenses/by/4.0/>).